Supplementary Materials for

Strengthened Influence of Atlantic Niño on ENSO in a Warming Climate

Lei Zhang[1,2,3*], Chunzai Wang[1,2,3*], Weiqing Han[4], Kristopher B. Karnauskas[4,5], Michael J. McPhaden[6], Aixue Hu[7], Wen Xing[1,2], Baiyang Chen[1,2], Heng Liu[1,2,8]

[1]State Key Laboratory of Tropical Oceanography, South China Sea Institute of Oceanology, Chinese Academy of Sciences, Guangdong, Guangzhou, China
[2]Global Ocean and Climate Research Center, South China Sea Institute of Oceanology, Chinese Academy of Sciences, Guangdong, Guangzhou, China
[3]Guangdong Key Laboratory of Ocean Remote Sensing, South China Sea Institute of Oceanology, Chinese Academy of Sciences, Guangzhou, China
[4]Department of Atmospheric and Oceanic Sciences, University of Colorado, Boulder, Colorado, USA
[5]Cooperative Institute for Research in Environmental Sciences, University of Colorado, Boulder, Colorado, USA
[6]National Oceanic and Atmospheric Administration/Pacific Marine Environmental Laboratory, Seattle, Washington, USA
[7]National Center for Atmospheric Research, Boulder, Colorado, USA
[8]University of Chinese Academy of Sciences, Beijing, China
**Corresponding authors. Emails: zhanglei@scsio.ac.cn; cwang@scsio.ac.cn*

This PDF file includes:

Table S1 List of climate models that participate in the Coupled Model Intercomparison Project Phase 6 (CMIP6) analyzed in this study. Monthly outputs from 149 members of 33 CMIP6 models were used. The analysis period is 1970–2100. In one member of CAS-ESM2-0 and two members of FGOALS-f3-L, only SST data is analyzed due to the unavailability of other key variables for the analysis period.

Model	# of ensemble members
ACCESS-CM2	10
ACCESS-ESM1-5	40
BCC-CSM2-MR	1
CanESM5	25
CanESM5-1	10
CanESM5-CanOE	3
CAS-ESM2-0	2
CESM2	3
CESM2-WACCM	3
CMCC-CM2-SR5	1
CMCC-ESM2	1
E3SM-1-1	1
EC-Earth3	2
EC-Earth3-CC	1
EC-Earth3-Veg	3
EC-Earth3-Veg-LR	3
FGOALS-f3-L	3
FGOALS-g3	4
FIO-ESM-2-0	1
GFDL-CM4	1
GFDL-ESM4	1
INM-CM4-8	1
INM-CM5-0	1
IPSL-CM6A-LR	7
KACE-1-0-G	1
KIOST-ESM	1
MIROC6	3
MPI-ESM1-2-HR	2
MPI-ESM1-2-LR	10
MRI-ESM2-0	1
NorESM2-LM	1
NorESM2-MM	1
TaiESM1	1

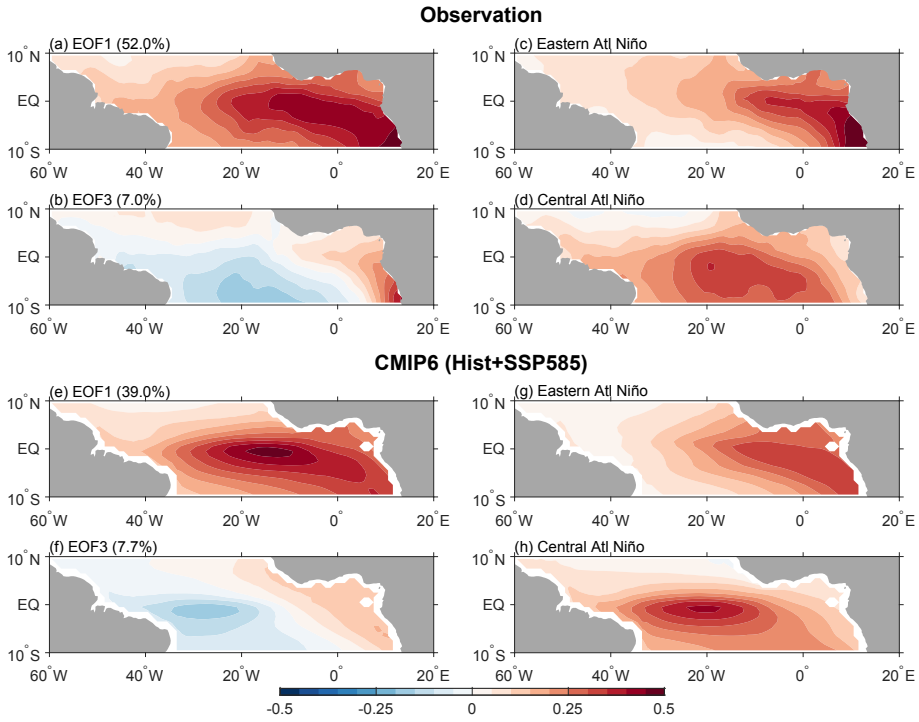

Figure S1 (a)(b) The first and third empirical orthogonal function (EOF) modes of sea surface temperature anomalies (SSTAs) in the tropical Atlantic during 1970–2022 from HadISST. The explained variance is shown in the parenthesis. (c)(d) The eastern (EAN) and central Atlantic Niño (CAN) patterns defined as (EOF1+EOF3)/√2 and (EOF1–EOF3)/√2, respectively. (e)–(h) As in (a)–(d), except for the average of CMIP6 model results during 1970–2100. Shown are average of 31 models that can well capture the observed EOF1 pattern (Fig. 2a). The influence of the anthropogenic global warming has been removed (see Methods).

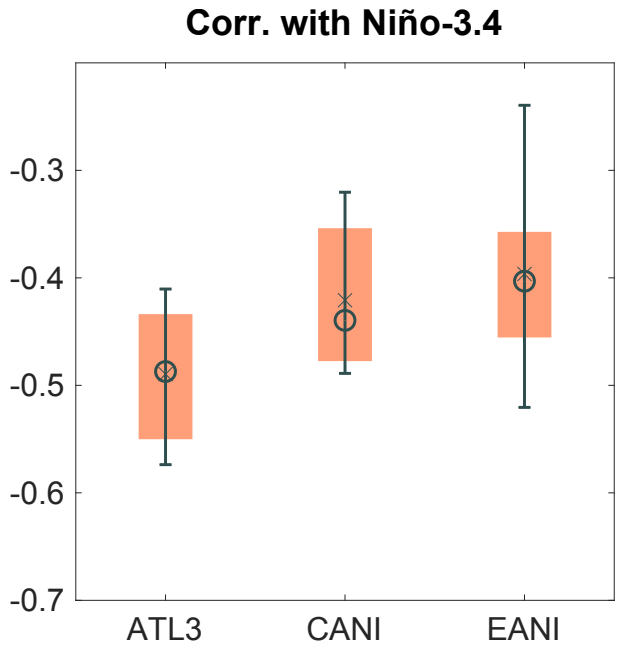

Figure S2 Boxplots of 21-year running correlation coefficients between December-January-February (DJF)-mean Niño-3.4 index and various JJA-mean Atlantic Niño indices in observations. The three columns represent results for ATL3, CANI, and EANI, respectively. Circles and cross signs represent the median and mean values, respectively. Error bars denote 25^{th} to 75^{th} percentiles, and vertical lines denote 10^{th} to 90^{th} percentiles.

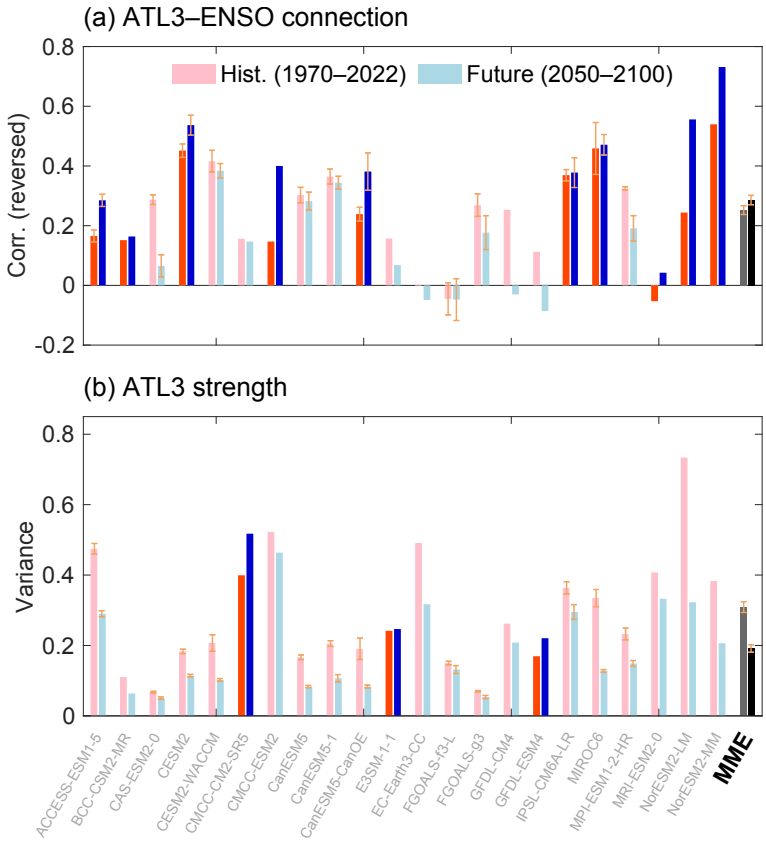

47

48 **Figure S3** (a) The ATL3–ENSO correlation during the historical period (red) and future
49 projections (blue) in the selected CMIP6 models (Fig. 2). The correlation coefficient is between
50 June-July-August (JJA)-mean ATL3 and December-January-February (DJF)-mean Niño-3.4
51 index, with the sign reversed. 10 out of 22 models simulate stronger ATL3–ENSO correlations,
52 which are shown in dark colors. Error bars represent uncertainties across different model
53 members (with at least 2 members) obtained through bootstrapping tests (see Methods). Multi-
54 member mean (MME) results during the historical period (gray) and future projections (black)
55 are shown in the last column, with mean values and error bars assessed based on 115 members
56 of 22 selected models. (b) As in (a), but for the ATL3 variance. Units are $^{\circ}C^2$.

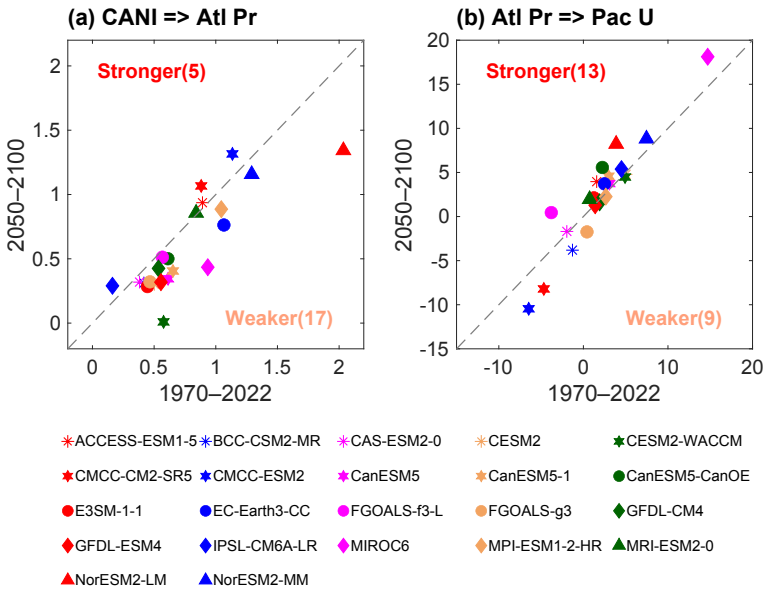

Figure S4 (a) Scatter plot of the regression of JJA-mean Atlantic rainfall anomalies (40˚W–10˚W, 5˚S–5˚N) on the normalized JJA-mean CANI during the historical period (1970–2022) against the future projections (2050–2100) in the selected CMIP6 models. Units are mm day^{-1}. (b) As in (a), except for the regression of the JJA-mean surface zonal wind stress anomalies over the tropical Pacific (150˚E–150˚W, 5˚S–5˚N) on the normalized JJA-mean Atlantic rainfall anomalies. Units are 10^{-3} N m^{-2}. The sign is flipped.

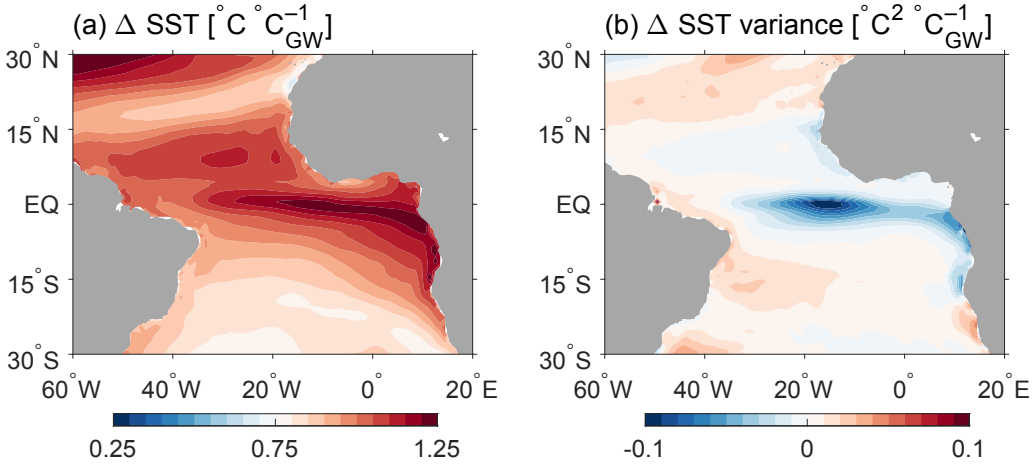

Figure S5 (a) Differences of JJA-mean SSTAs between the historical period and future projections (future minus historical). Units are ˚C ˚C^{-1}. Note that the global mean SST warming is retained in the figure, different from Figure 5a. (b) As in (a), except for the differences of the variance of JJA-mean SSTAs. Units are ˚C^2 ˚C^{-1}. Both changes are scaled by the global mean SST warming during boreal summer in each model member prior to calculating the ensemble averages.

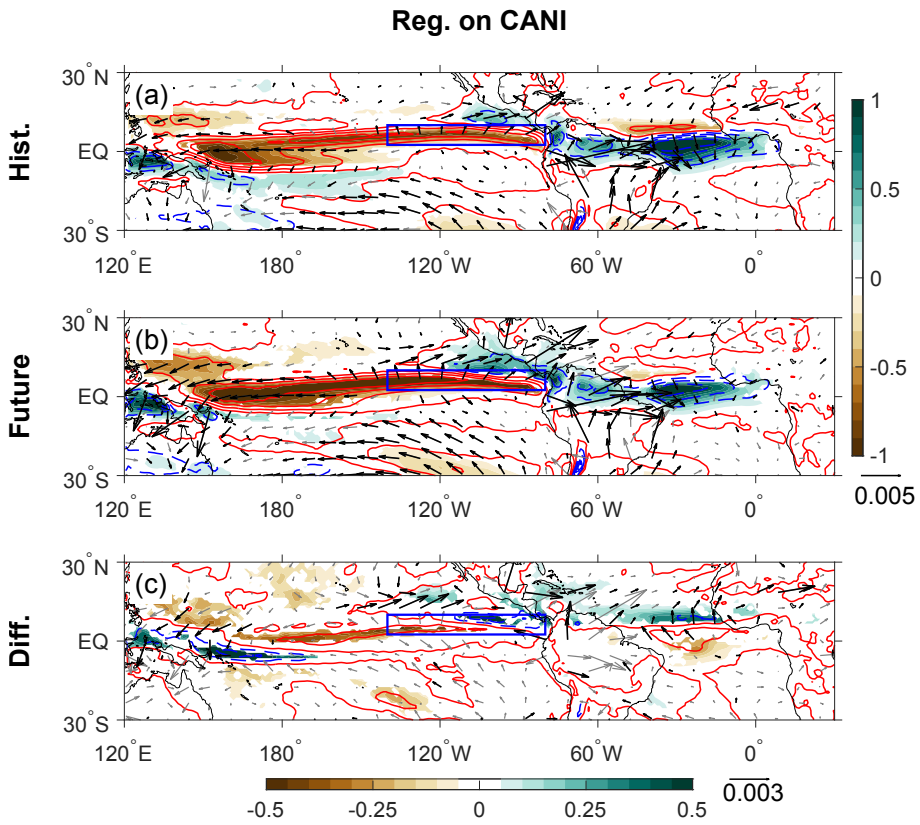

71

72 **Figure S6** (a) Regression of JJA-mean precipitation (shading, mm day^{-1}), surface wind stress
73 (N m^{-2}), and 500 hPa omega (contour, 10^{-2} Pa s^{-1}) anomalies on the normalized JJA-mean
74 CANI during the historical period. Shown are averaged results from the selected CMIP6
75 models. (b) As in (a), except for future projections. (c) Differences between (a) and (b). The
76 blue box denotes the Pacific Intertropical Convergence Zone (ITCZ) (140°W–80°W, 2.5°N–
77 10°N). Shading and black vectors denote results for which more than 70% of the models agree
78 with the signs of changes.

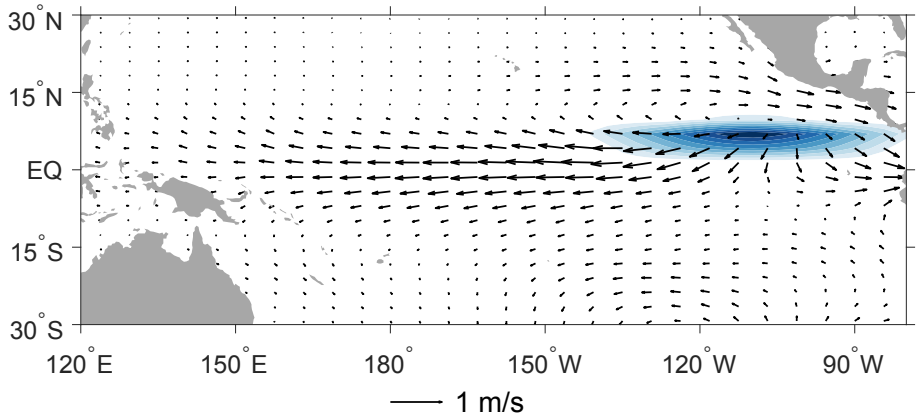

Figure S7 850hPa wind anomalies (vectors, m s^{-1}) simulated by the Linear Baroclinic Model (LBM), driven by the heating anomalies in the eastern Pacific ITCZ region (shading) during boreal summer (see Methods).

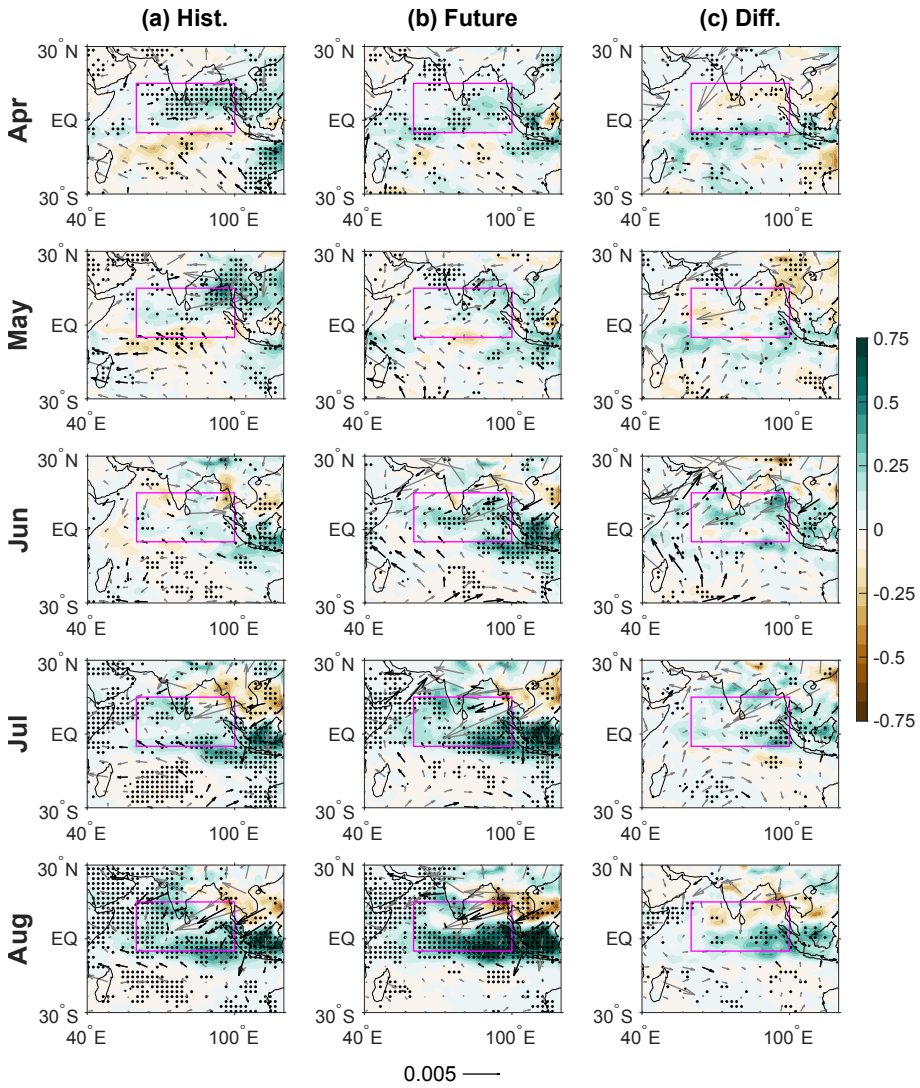

Figure S8 (a) Regression of monthly (April–August) rainfall (shading, mm day^{-1}) and surface wind stress (vector, 10^{-2} Pa s^{-1}) anomalies on the normalized JJA-mean CANI during the historical period. (b) As in (a), except for future projections. (c) Differences between (a) and (b). Stippling and black vectors denote results for which more than 70% of the models agree with the signs of changes. The boxes denote the region where pronounced rainfall changes occur (60˚E–100˚E, 5˚S–15˚N) (see Figs. S10 and S11).

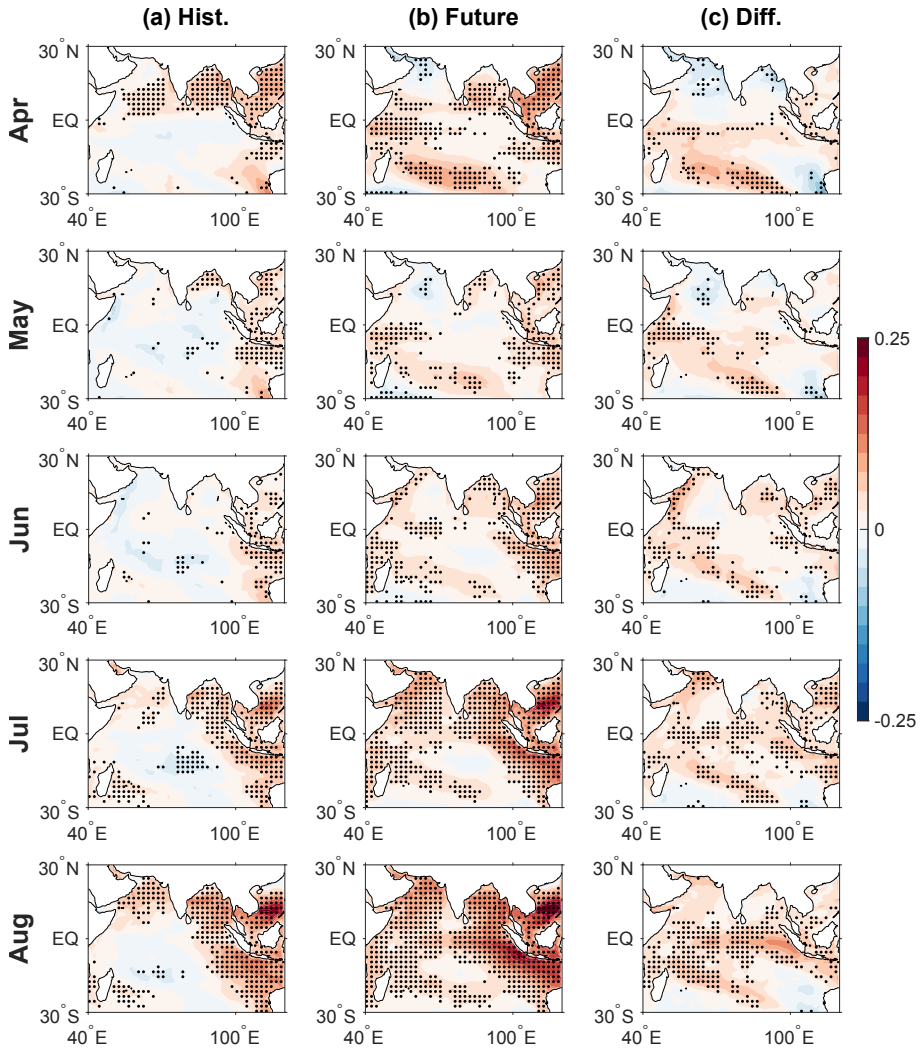

Figure S9 As in Fig. S8, except for regression of monthly SST anomalies. Unit is ˚C.

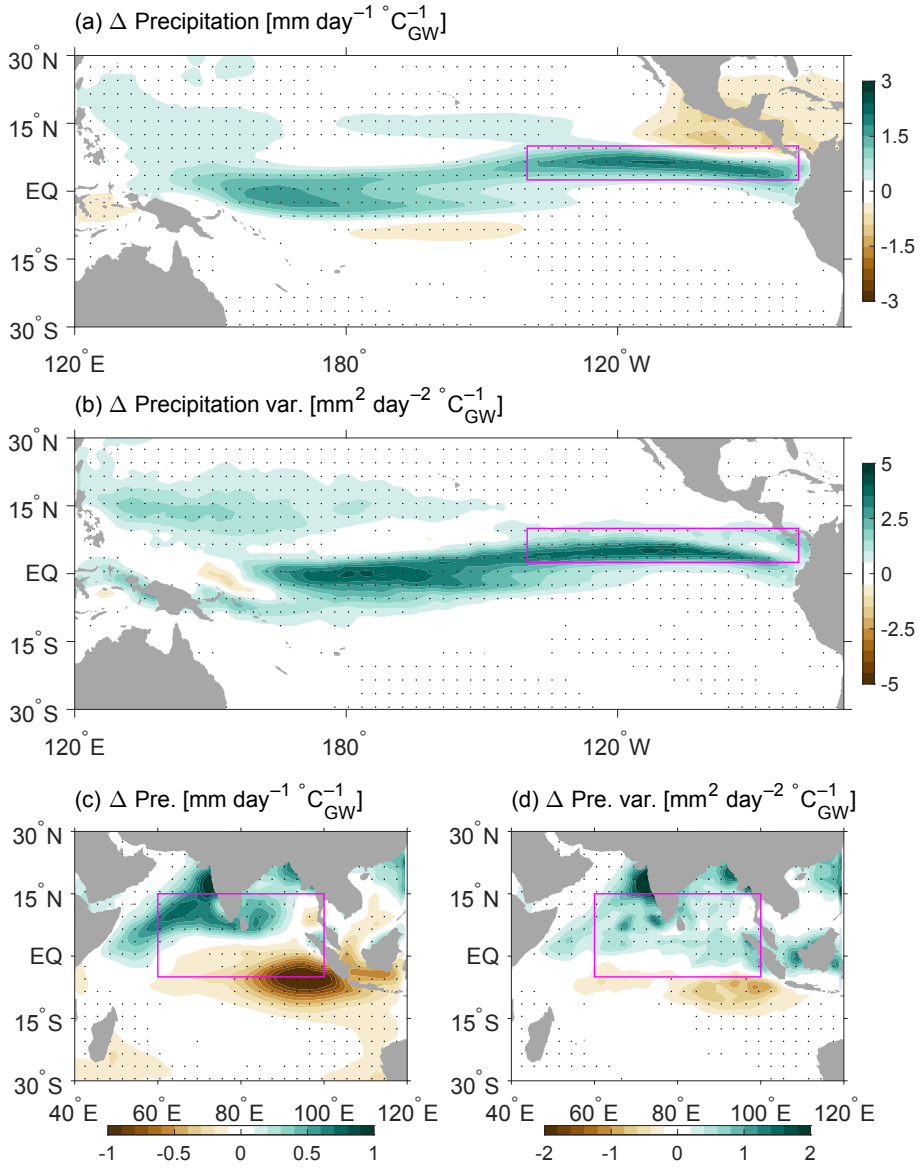

Figure S10 (a) Shading denotes differences of the JJA-mean precipitation between the historical simulations and future projections in the selected CMIP6 models. Units are mm day^{-1} °C^{-1}. The magenta box denotes the Pacific ITCZ (140°W–80°W, 2.5°N–10°N). (b) As in (a), except for changes in the variance of JJA-mean precipitation anomalies. Units are mm^2 day^{-2} °C^{-1}. Changes in (a) and (b) are scaled by the global mean SST warming during boreal summer in each model member prior to calculating the ensemble averages. Stippling denotes the regions where more than 70% of the models agree with the sign of changes. (c)(d) As in (a)(b), except for the tropical Indian Ocean region. The box region is 60°E–100°E, 5°S–15°N.

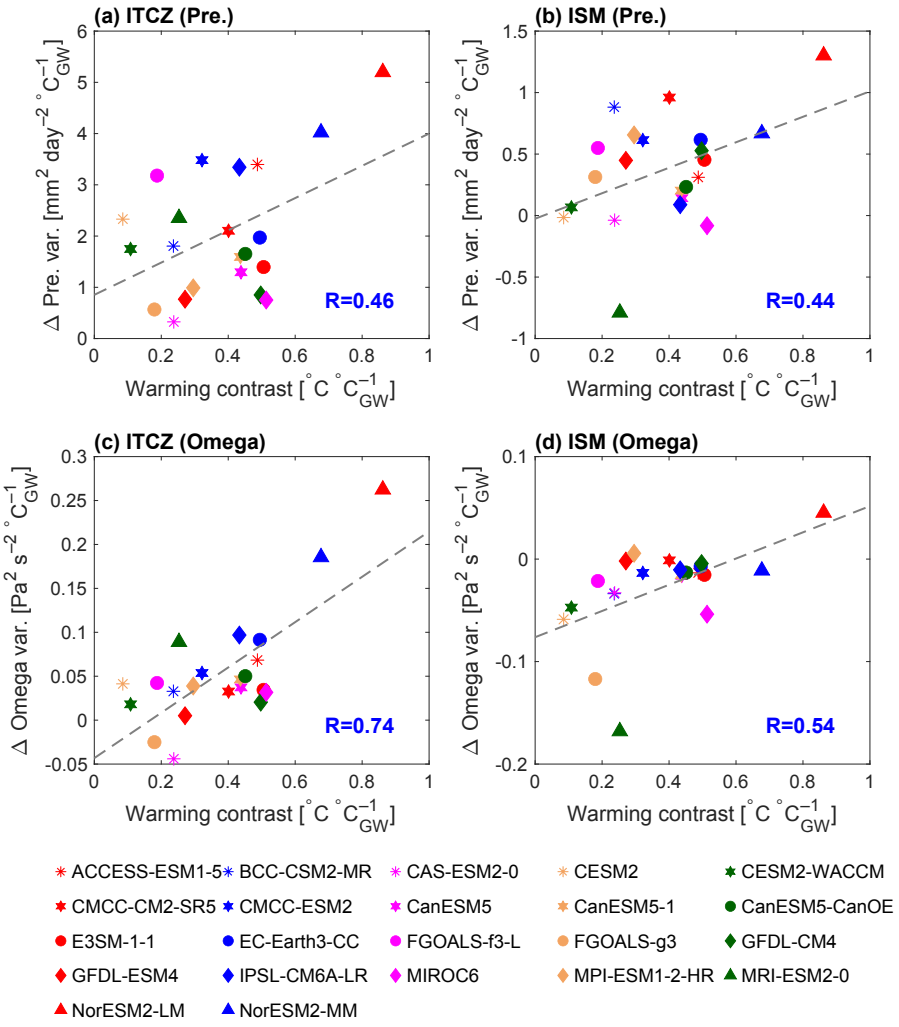

Figure S11 (a) Scatter plot of the JJA-mean interhemispheric warming contrast in future projections compared to the historical period against changes in the variance of JJA-mean precipitation anomalies over the eastern Pacific ITCZ region (140°W–80°W, 2.5°–10°N, mm^2 day^{-2} °C^{-1}) in the selected CMIP6 models. The dashed line denotes the linear regression between the two, and their correlation is shown at the lower right corner (P<0.05). The warming contrast is defined as differences of SST warming between the Northern (0°–60°N) and Southern Hemisphere (60°S–0°). (b) As in (a), except that the y-axis shows changes in the variance of JJA-mean precipitation anomalies over the North Indian Ocean (60°E–100°E, 5°S–15°N). (c)(d) As in (a)(b), except that the y-axis shows changes in the variance of JJA-mean 500hPa omega over the two regions (10^{-3} Pa^2 s^{-2} °C^{-1}).

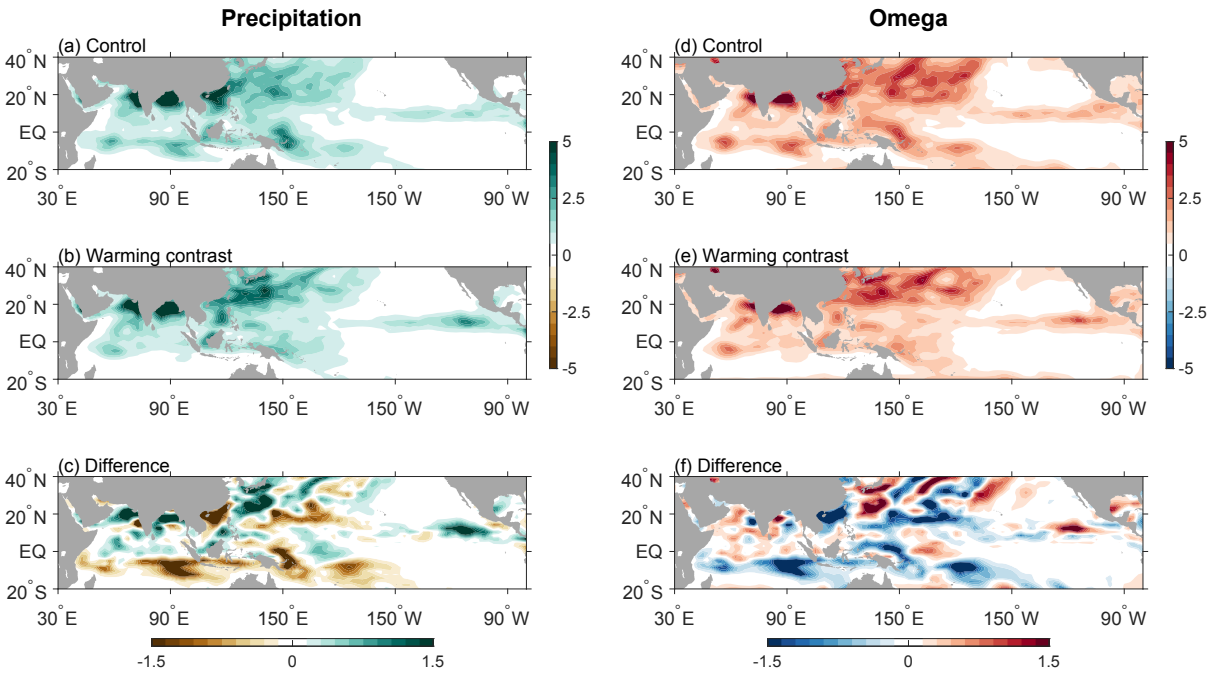

Figure S12 (a) Variance of JJA-mean rainfall anomalies in the control simulation forced with monthly SST climatology. Units are $mm^2\ day^{-2}$. (b) As in (a), except for results from the sensitivity experiment forced with 1˚C uniform SST warming in the Northern Hemisphere (see Methods). (c) Differences between (b) and (a). The two boxes denote the Pacific ITCZ region (140˚W–80˚W, 2.5˚–10˚N) and North Indian Ocean (60˚E–100˚E, 5˚S–15˚N). (d)–(f) As in (a)–(c), except for variance of 500hPa omega anomalies ($10^{-4}\ Pa^2\ s^{-2}$).

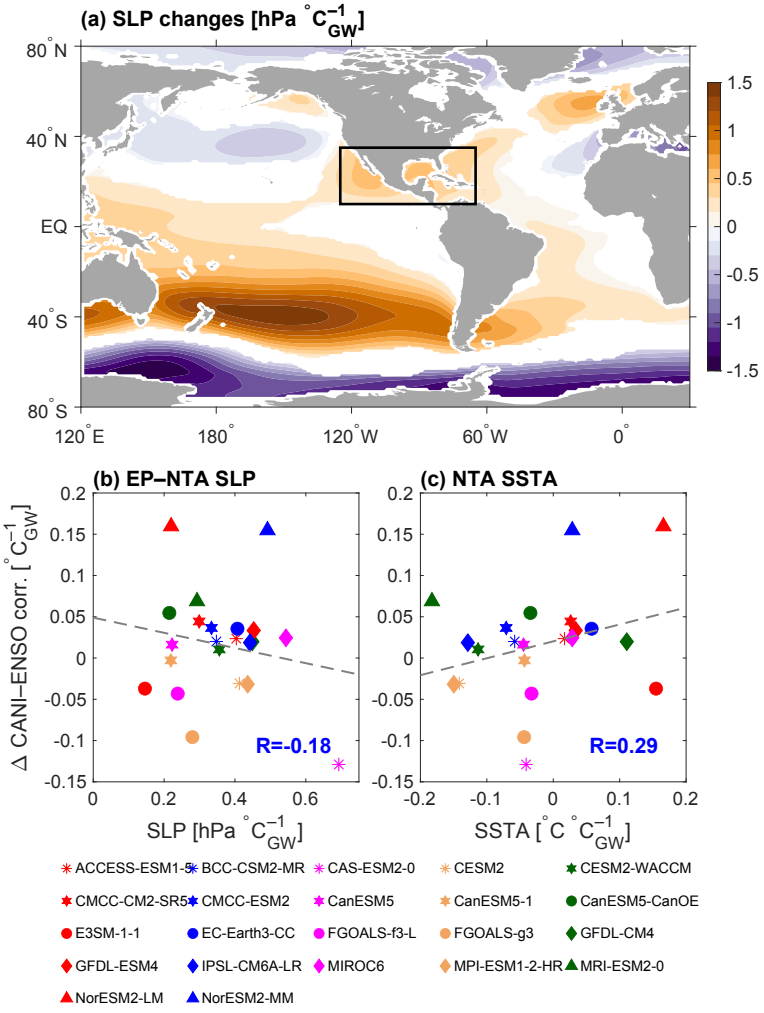

Figure S13 (a) Differences of JJA-mean sea level pressure (SLP, shading; hPa °C^{-1}) between the historical period and future projections in the 22 selected CMIP6 models (future minus historical). Shading denotes results for which more than 70% of the models agree with signs of changes. (b) Scatter plot of the eastern Pacific–North Atlantic SLP anomalies against changes in the CANI–ENSO correlation (sign flipped). The dashed line denotes the linear regression between the two, and their correlation is shown at the lower right corner. The SLP anomalies are averaged over the oceanic area within the black boxed region (125°W–65°W, 10°N–35°N). (c) The scatter plot of the North Atlantic SSTAs (80°W–20°W, 5°N–25°N) against changes in the CANI–ENSO correlation (sign flipped). The tropical mean warming between 30°S and 30°N was removed. Note that all changes are scaled by the global mean SST warming during boreal summer in each model member.

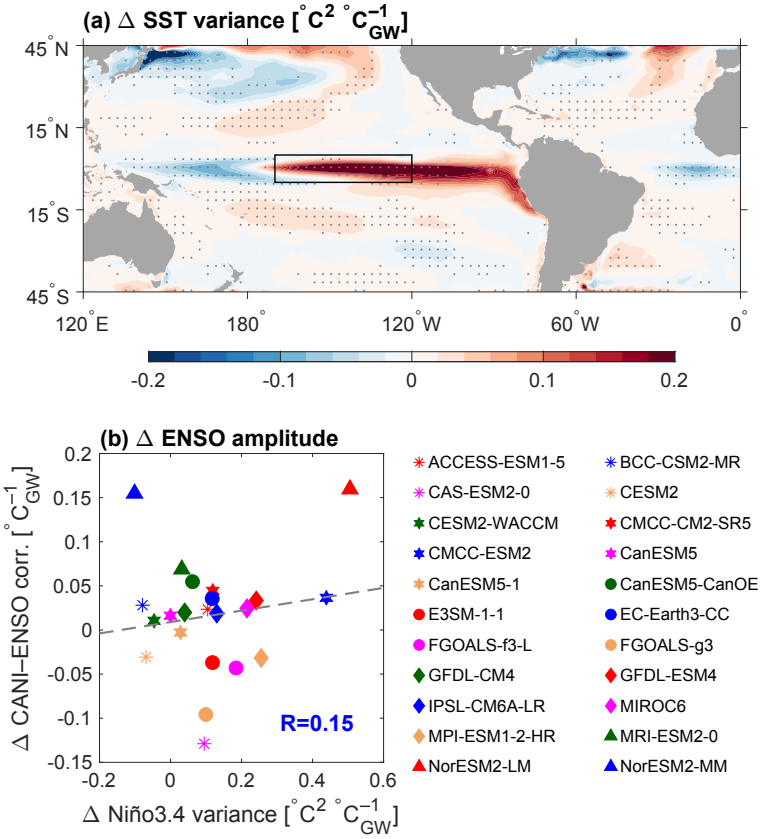

Figure S14 (a) Differences of JJA-mean SSTA variance (shading; $^{\circ}C^{2}$ $^{\circ}C^{-1}$) between the historical period and future projections in the 22 selected CMIP6 models (future minus historical). Stippling denotes the results for which more than 70% of the models agree with signs of changes. (b) Scatter plot of changes in the variance of JJA-mean SSTAs in the Niño-3.4 region (black box, 170°W–120°W, 5°S–5°N) against changes in the CANI–ENSO correlation (sign flipped). The dashed line denotes the linear regression between the two, and their correlation is shown at the lower right corner. All changes are scaled by the global mean SST warming during boreal summer in each model member.

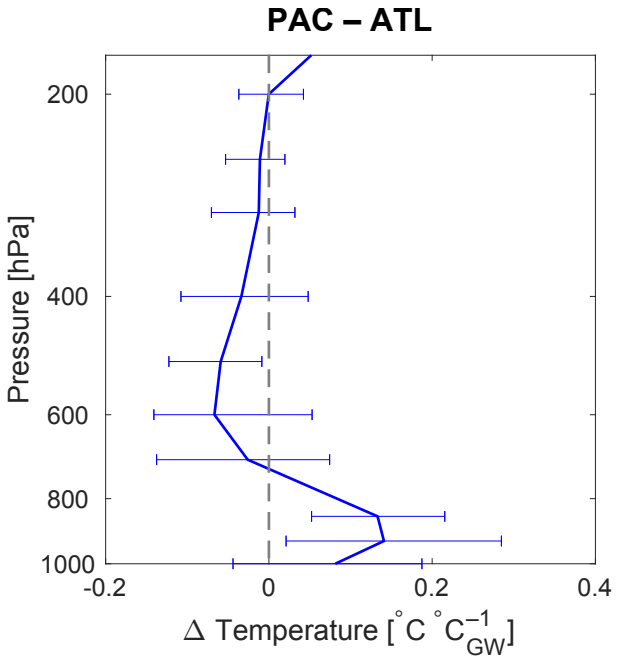

Figure S15 Differences of the JJA-mean tropospheric warming between the eastern tropical Pacific (120˚W–80˚W, 10˚S–10˚N) and Atlantic Oceans (50˚W–10˚W, 10˚S–10˚N). The tropospheric warming is defined as temperature changes between the historical period and future projections in the selected CMIP6 models (future minus historical). Units are ˚C ˚C^{-1}. Horizontal error bars denote the 15th and 85th percentiles across the selected CMIP6 models (see Methods). All changes are scaled by the global mean SST warming during boreal summer in each model member.

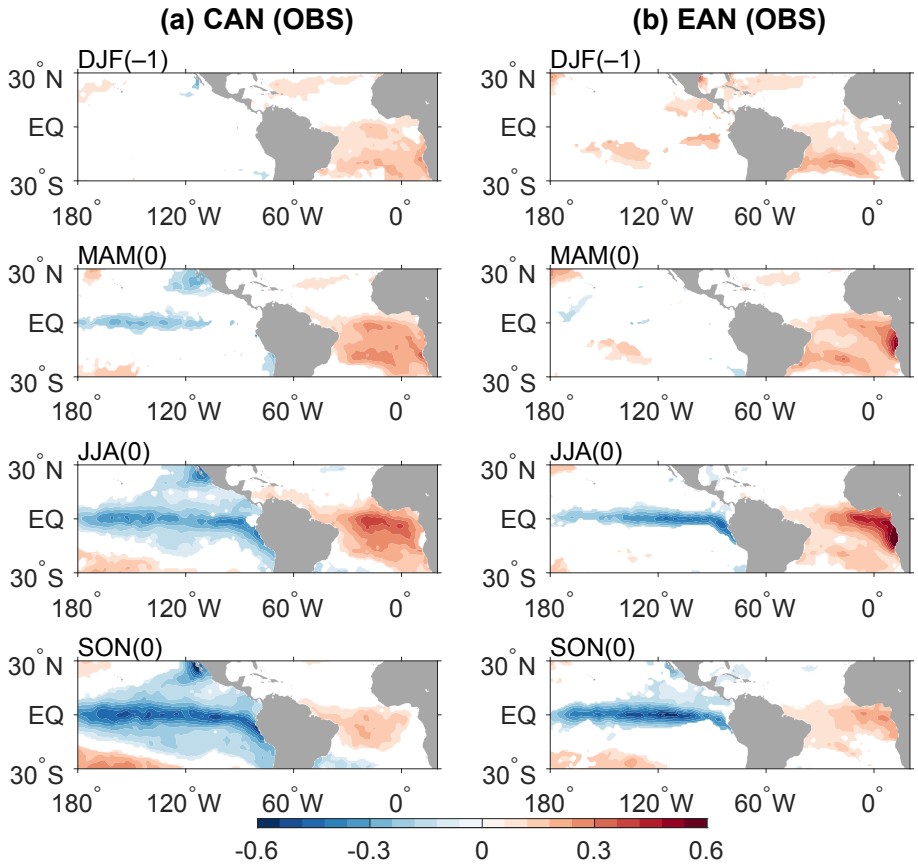

Figure S16 (a) Regression of seasonal mean SSTAs on the normalized JJA-mean CANI in observations. Shown are DJF-mean from the preceding winter, March-April-May (MAM)-mean, JJA-mean, and September-October-November (SON)-mean results. (b) As in (a), but for regression of SSTAs on normalized JJA-mean EANI. Unit is ˚C. Shown are results that are statistically significant at the 90% confidence level.

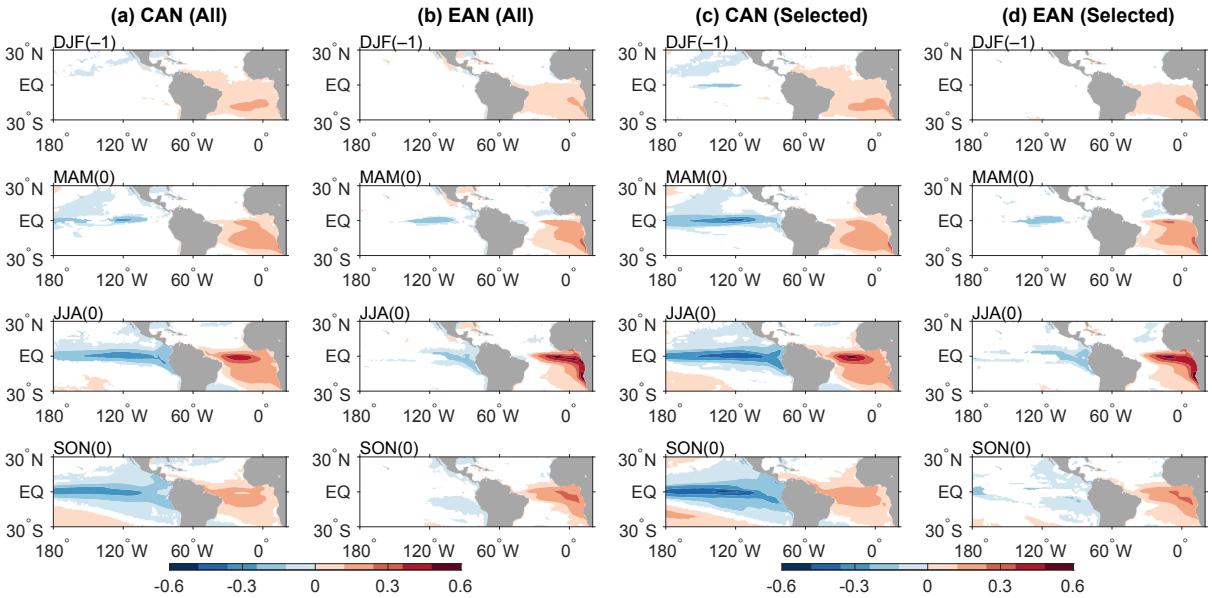

Figure S17 As in Figure S16, but for CMIP6 results. (a)(b) Average of all CMIP6 models. (c)(d) Average of the 22 selected models (see Figure 2). Shown are results for which more than 70% of the models agree with the signs of changes.